

## Conically degenerate anchoring effect in planar nematic-liquid-crystal shells

Seyed Reza Seyednejad<sup>1,\*</sup> and Mohammad Reza Mozaffari<sup>2,†</sup>

<sup>1</sup>*Institute for Advanced Studies in Basic Sciences, Zanjan 45195-159, Iran*

<sup>2</sup>*Department of Physics, University of Qom, Qom 3716146611, Iran*



(Received 15 March 2021; accepted 10 June 2021; published 1 July 2021)

We study the defect texture in symmetric and asymmetric states of a nematic-liquid-crystal shell with conic and planar degenerate surface anchorings on the inner and outer spherical boundaries, respectively. To achieve the equilibrium nematic orientation, we numerically minimize the Landau–de Gennes free energy by employing surface potentials on the shell walls. The symmetric nematic shells energetically have stable configurations independent of thickness. In thick shells, the director field satisfies bipolar and hexadecapolar configurations between boundaries. In thin shells, the boojums transform into two stable disclination curves.

DOI: [10.1103/PhysRevE.104.014701](https://doi.org/10.1103/PhysRevE.104.014701)

### I. INTRODUCTION

Developments in microfluidic devices to fabricate spherical shells of nematic liquid crystal (NLC) have raised hopes for using polymer linkers in photonic applications [1,2], although controlling the binding sites on the vertices of defects is chemically heavy duty [3]. The nematic defect structures and their stability in such colloids are the critical contents in this context [4–13].

Nematic molecule behavior on the shell surfaces distorts the local order in the confined nematic layer and regions appear as points and/or lines with zero nematic ordering which depend on the thickness, asymmetry degree, and inner and outer surface coatings [14–20]. The average orientation of elongated nematic molecules locally specifies a preferred direction that is called the director. The director is a unit vector with headless symmetry ( $\hat{n} \equiv -\hat{n}$ ). Defects are topologically related to regions where the director distorts due to the surface coating that is well known as anchoring or external fields [21]. The surface anchoring depends on the orientation of the nematic mesogens on the boundaries and their strength, with preferred (normal) or degenerate (planar and conical) configurations [4,22–27].

In strong normal anchoring on the spherical surface, the elastic quadrupole symmetry induces a Saturn ring with strength  $s = -1/2$  that encircles the colloid at the equator. In weak normal anchoring, the dipole symmetry deviation leads to a hyperbolic hedgehog point defect ( $s = -1$ ) that appears near the particle inside the bulk [4,28]. The nematic droplets show the same singularities with different winding signs [26,29].

Degenerate planar anchoring on the spherical surface leads to bipolar symmetry with a pair of boojums ( $s = +1$ ) at the poles of the particle in bulk [22]. The bipolar defect texture is also observed in the nematic droplets [30,31]. The

Poincaré-Hopf theorem indicates that the total topological charge on a spherical nematic shell with tangential boundary condition is equal to  $+2$  [32,33]. Depending on the shell thickness, the elastic distortions show two defect arrangements. The bipolar texture appears in thick shells with two paired boojums, and the tetrahedron configuration has emerged in thin shells with four disclination lines ( $s = +1/2$ ) [5,6,17,34]. The defect textures of the nematic shells also depend on the external fields [20,35].

Conically degenerate anchoring on the spherical surface simultaneously induces a loop defect and a boojum pair similar to particles with perpendicular and planar anchorings. For a nematic droplet, the winding number of the loop defect is equal to  $+1/2$  [25,36], while it is  $-1/2$  for an immersed colloid in a nematic bulk [23,27,37]. This study numerically investigates symmetry and asymmetry of nematic-liquid-crystal shells with degenerate conic and planar surface anchorings on their inner and outer spherical boundaries, respectively.

### II. NUMERICAL METHOD

We have used a second rank, traceless, and symmetric tensor,  $Q_{ij}$ , to describe the confined nematic layer. The largest eigenvalue and its corresponding eigenvector of the nematic tensor are related to the scalar order parameter and director orientations. The equilibrium nematic order and orientation are obtained by minimizing the Landau–de Gennes free energy and surface planar and conical energies in terms of nematic tensor.

The Landau–de Gennes free energy in the uniaxial regime is given in terms of the nematic tensor order parameter and its spatial derivatives as

$$\mathcal{F}_{\text{LDG}} = \int_{\Omega} dV \left( \frac{a_0 \Delta T}{2} Q_{ij} Q_{ji} - \frac{B}{3} Q_{ij} Q_{jk} Q_{ki} + \frac{C}{4} (Q_{ij} Q_{ji})^2 + \frac{L_1}{2} \partial_k Q_{ij} \partial_k Q_{ij} \right), \quad (1)$$

\*seiednejad@gmail.com

†m.mozaffari@qom.ac.ir

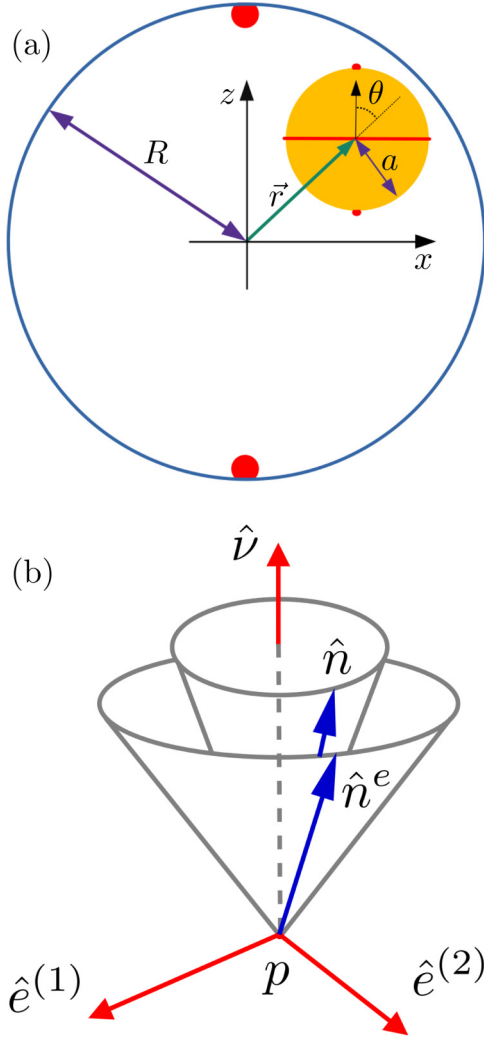


FIG. 1. (a) Schematic defect structure inside a nematic spherical shell.  $R = 0.5 \mu\text{m}$  and  $a$  are the radii of outer and inner spheres, respectively,  $\vec{r}$  shows the center-to-center distance vector of the two spheres, and  $\theta$  expresses the polar angle of  $\vec{r}$  with respect to the  $z$  axis. Axis  $z$  is determined by the normal vector of the surface containing the saturn ring defect around the inner sphere shown by red color. Boojum defects on both surfaces are also shown by red dots. (b) A schematic of the conically degenerate anchoring. Equilibrium direction  $\hat{n}^e$  freely can rotate on a cone with the vertex angle  $\psi_c = 45^\circ$ . Surface normal vector  $\hat{v} (= \hat{e}^{(1)} \times \hat{e}^{(2)})$  defines a right-handed coordinate system in which the  $\hat{e}^{(2)}$  axis lies in the plane surface of  $\hat{v}$  and  $\hat{n}$ .

where  $\int_{\Omega} dV$  represents integrating over the space filled by the NLC. The indices refer to the Cartesian coordinates; the Einstein summation convention is assumed [38]. The first three terms describe the isotropic-nematic phase transition. Positive coefficients  $a_0$ ,  $B$ , and  $C$  depend on the NLC material and  $\Delta T = T - T^*$ , where  $T^*$  is the nematic supercooling temperature. The bulk scalar order parameter in the uniform nematic phase is given by  $S_b = (B/6C)(1 + \sqrt{1 - 24a_0\Delta TC/B^2})$ . The last term is the contribution of elastic distortions in one-constant approximation with coefficient  $L_1$ . Frank elastic moduli are related to the above parameters as  $K_{\text{splay}} = K_{\text{twist}} = K_{\text{bend}} = 9L_1S_b^2/2$ . We use the

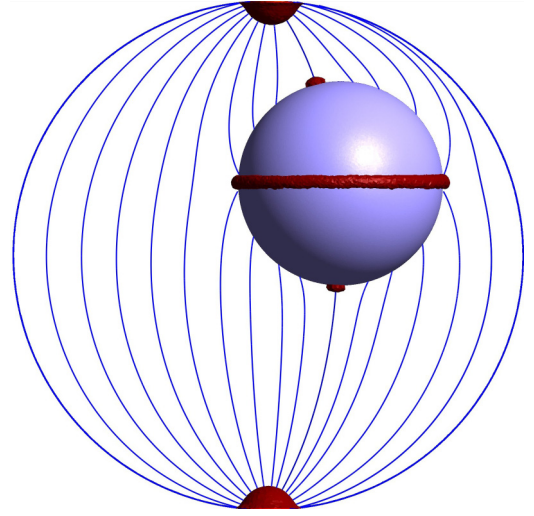


FIG. 2. General director field and defect structure of the shell with heterogeneous thickness.

5CB nematic parameters ( $a_0 = 0.087 \times 10^6 \text{ J/m}^3 \text{ K}$ ,  $T^* = 307.15 \text{ K}$ ,  $T = 305.17 \text{ K}$ ,  $B = 2.12 \times 10^6 \text{ J/m}^3$ ,  $C = 1.73 \times 10^6 \text{ J/m}^3$ ,  $L_1 = 4 \times 10^{-11} \text{ J/m}$ ) [39,40].

A schematic of the considered geometry is given in Fig. 1(a). The nematic shell has been confined with two spherical surfaces. The shell radii in the inner and outer boundaries are  $a$  and  $R$ , respectively. We scale all the lengths with the outer radius  $R = 0.5 \mu\text{m}$ . The inner core is spatially specified by  $r$  and  $\theta$  concerning the center of the outer sphere. The inner and outer boundaries have degenerate conic and planar anchorings, respectively. To this end, we introduce the surface energies in terms of the nematic tensor as

$$\mathcal{F}_S = \frac{W_1}{2} \int_{\text{inner}} dS (Q_{ij} - Q_{ij}^e)(Q_{ji} - Q_{ji}^e) + W_2 \int_{\text{outer}} dS (\tilde{Q}_{ij} - \tilde{Q}_{ij}^\perp)(\tilde{Q}_{ji} - \tilde{Q}_{ji}^\perp). \quad (2)$$

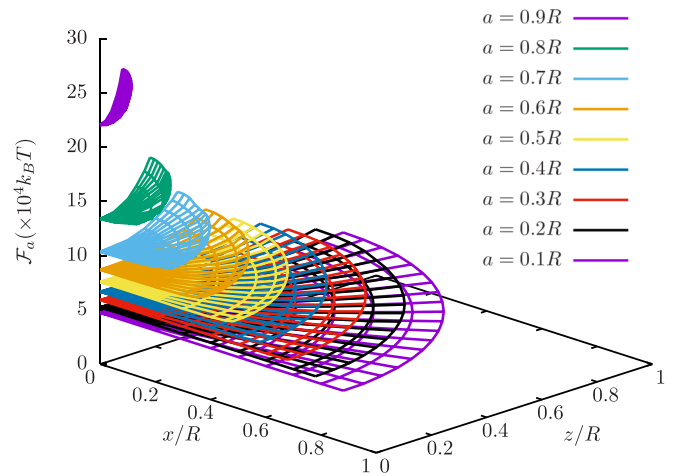


FIG. 3. Total free energy  $\mathcal{F}_a(\vec{r})$  dependence on off-center displacement vector  $\vec{r}$  of the inner sphere for different amounts of radius  $a$ .

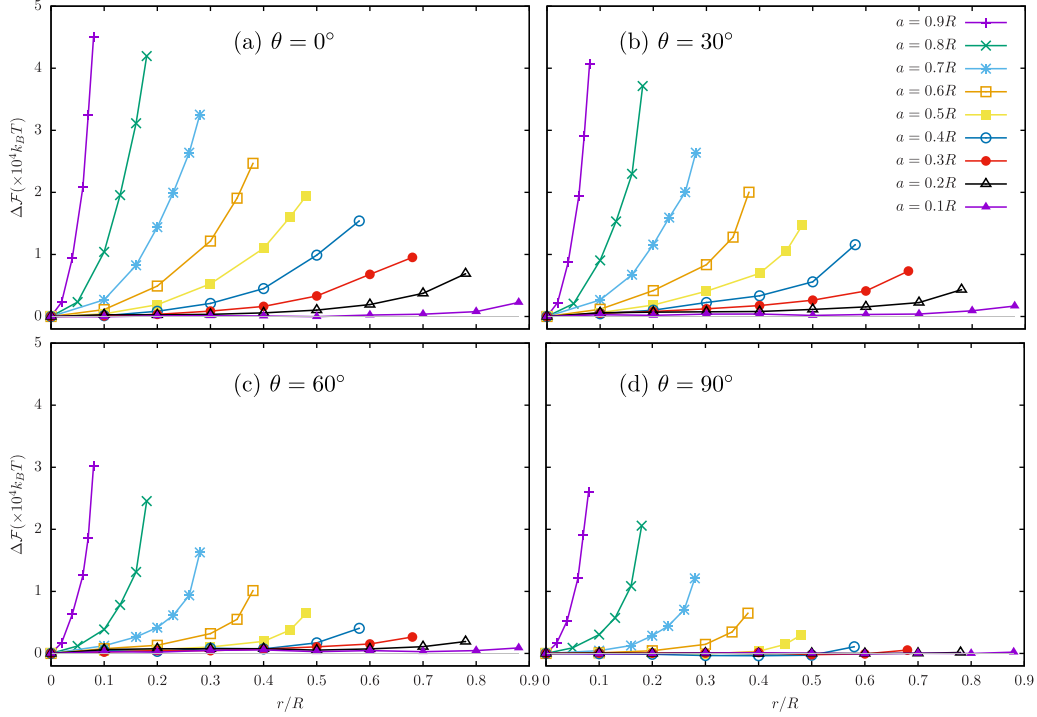


FIG. 4. Free energy dependence on the off-center displacement at various amounts of  $a$  with (a)  $\theta = 0^\circ$ , (b)  $\theta = 30^\circ$ , (c)  $\theta = 60^\circ$ , and (d)  $\theta = 90^\circ$ . Free energy difference is defined as  $\Delta\mathcal{F} = \mathcal{F}_a(\bar{r}) - \mathcal{F}_a(0)$ .

The first term satisfies degenerate conical anchoring on the inner surface where the equilibrium tensor  $Q_{ij}^e = S_b(3\hat{n}_i^e\hat{n}_j^e - \delta_{ij})/2$  is locally determined by the equilibrium conical orientation,  $\hat{n}^e = \hat{v} \cos \psi_e + \hat{e}^{(2)} \sin \psi_e$ , on the surface. The equilibrium director orientation  $\hat{n}^e$  locally makes an equilibrium conic angle  $\psi_e = 45^\circ$  with the surface normal vector  $\hat{v}$  [see Fig. 1(b)] [37]. The second term satisfies degenerate planar anchoring on the outer surface, where  $\tilde{Q}_{ij} = Q_{ij} + S\delta_{ij}/2$  and  $\tilde{Q}_{ij}^\perp = (\delta_{ik} - \hat{v}_i\hat{v}_k)\tilde{Q}_{kl}(\delta_{lj} - \hat{v}_l\hat{v}_j)$  are uniaxial parallel and projection tensors, respectively [41]. The anchoring strengths are assumed to be in the strong regime as  $W_1 = 5 \times 10^{-3} \text{ J/m}^2$  and  $W_2 = 10^{-2} \text{ J/m}^2$ .

We have numerically used the finite element method (FEM) to minimize the total free energy ( $\mathcal{F} = \mathcal{F}_{\text{LdG}} + \mathcal{F}_S$ ) [11]. An automatic mesh generator has been employed to discretize the nematic layer into tetrahedral elements [42]. The nematic tensor is approximated as linear. The interpolation validity depends on the deviations of nematic tensor inside of each element, which can be improved by adjusting the size of elements. In this study we chose the average element size  $L_e \simeq 0.01R$  all over the shell. We use the conjugate gradient method for minimizing the dimensionless free energy where iteration stops when the free energy difference between the steps shows a value smaller than  $10^{-10}$  [43].

### III. RESULTS AND DISCUSSION

Firstly we have considered an asymmetric shell to evaluate the operation of surface energies on the inner and outer shell boundaries. Figure 2 satisfies our elementary expectations. The nematic layer indicates a pair of boojums on the outer surface while simultaneously including a pair of boojums

and a Saturn ring defect on the inner surface. The director deformations follow both bipolar defect texture [30] and hexadecapolar director configuration [23] around the outer and inner surfaces, respectively. Although the disclination loop does not move around, the point defects on the inner shell show small displacements. We have found the same behavior in thick asymmetric shells.

We have geometrically defined a reference coordinate system based on that shown in Fig. 1(a), where the  $z$  axis is parallel with the normal vector of the Saturn ring plane surface and the  $x$ - $z$  plane includes the centers of both spherical surfaces.

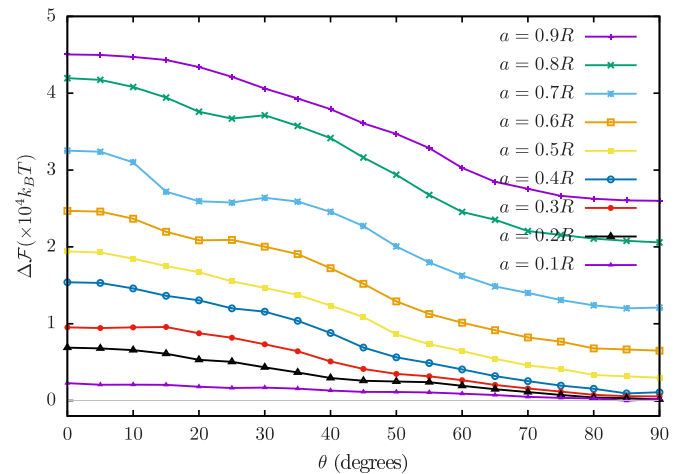


FIG. 5. Maximum free energy values at maximum amounts of  $r$  varying with  $\theta$ . Inner sphere is nearly touching the wall of the outer sphere.

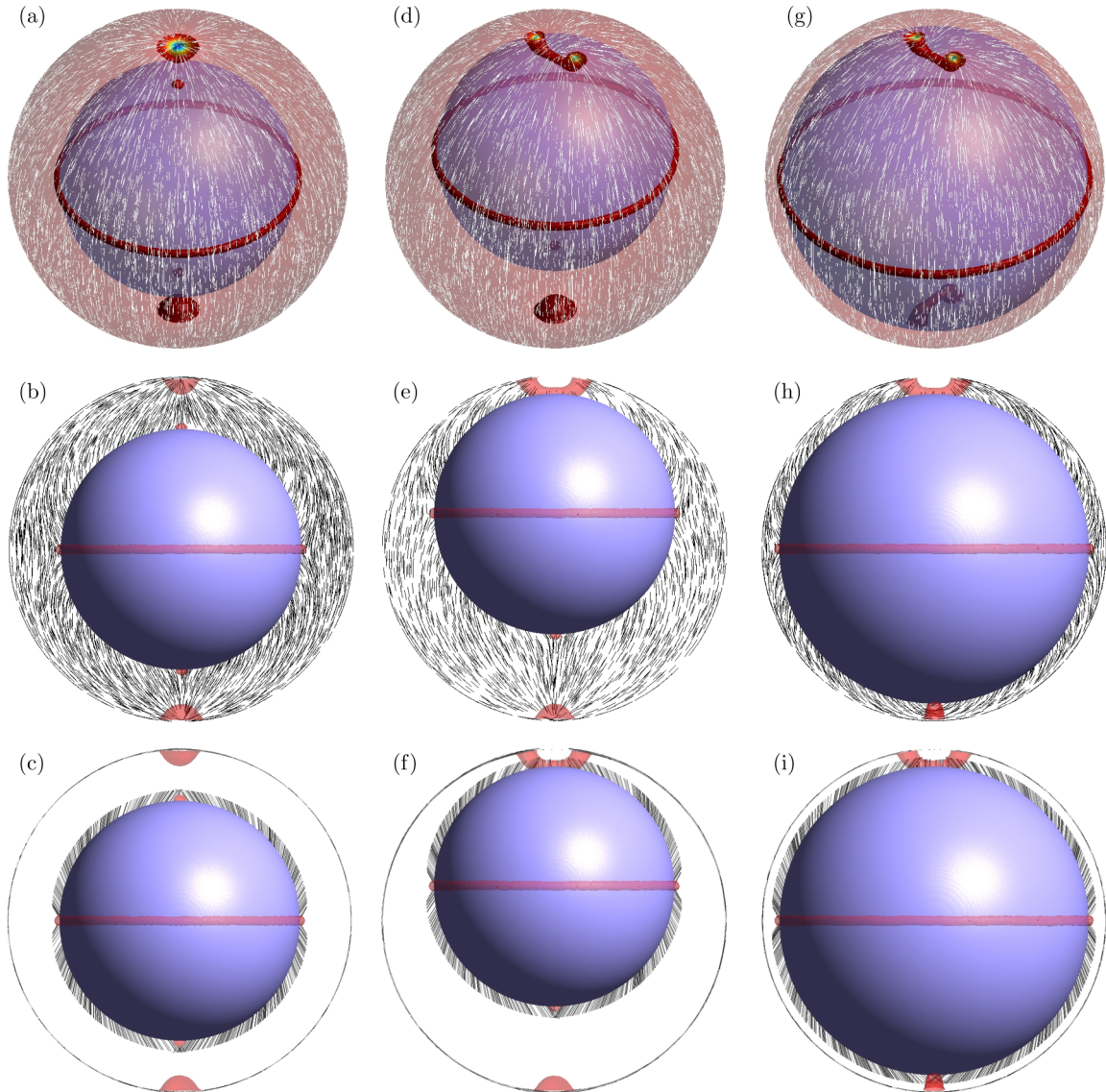


FIG. 6. Possible defect structures of NLC shells with conically degenerate and degenerate planar anchorings on inner and outer surfaces, respectively: (a)–(c) boojums bipolar structure on a symmetric thick shell with  $a = 0.7R$ , (d)–(f) triangular defect texture on a highly asymmetric shell with  $a = 0.7R$ ,  $r = 0.2R$ , and  $\theta = 0$ , and (g)–(i) tetrahedral defect structure in a very thin symmetric shell where  $a = 0.9R$ . The first row shows defect structures and planar director field on the outer surface. The second and third rows show a cross section of the director field inside the bulk and on the shell surfaces, respectively.

Figure 3 energetically explains the inner core treatment as a function of geometrical parameters. Each point in the three-dimensional (3D) plot shows an independent numeric calculation. The energy landscape denotes that the inner core tends to maintain its symmetric state. It shows that the core moving toward the outer surface increases the free energy. For a better insight, we define the free energy difference as  $\Delta\mathcal{F} = \mathcal{F}_a(\bar{r}) - \mathcal{F}_a(0)$ , which removes the reference of energy in each radius of the inner core. Figures 4(a)–4(d) represent more precisely that the shell is stable, since the cost of elastic deformations prevents the shell destruction in the absence of surface tension. The arrangement of defects in the  $z$  axis at the poles of an asymmetric shell for  $\theta = 0^\circ$  [Fig. 4(a)] causes the director to feel strong distortions with respect to the  $\theta = 90^\circ$  case [Fig. 4(d)].

Slopes of the energy-displacement curves in Fig. 4 can describe the mobility of the inner core around the symmetric configuration, although we have not calculated the hydrodynamics effect. In the presence of thermal fluctuations, the thick shells can exhibit more freedom compared to the thin shells.

Figure 5 illustrates the surface close contact interactions. It includes the maximum free energy difference when the inner core nearly touches the outer surface. The plots can be treated as energy barriers when the inner core displaces from  $\theta = 90^\circ$  to  $\theta = 0^\circ$ . As shown in Fig. 5, the height of barriers increases with decreasing the thickness of the nematic shell, which varies from  $10k_B T$  (at  $a = 0.1R$  and  $\theta = 90^\circ$ ) to  $10^4 k_B T$  (at  $a = 0.9R$  and  $\theta = 0^\circ$ ) in order of magnitude at room temperature.

The stable location of the inner core interestingly shows inconsistent results when the shell surfaces have the planar-planar and conical-planar anchorings. The inner core tends to move out of the center and locate as close as possible to the outer shell wall in planar-planar anchoring, while in conical-planar anchoring, the inner core will keep its spatial symmetric configuration. When the two spheres are almost tangent (for a distance  $d \rightarrow 0$ ), the main distortion is localized between the sphere surfaces (due to the anchoring incompatibility) with a typical energy density of order  $(K/2)(\Delta\phi/d)^2$ , which repels the inner core but only when the difference of anchoring  $\Delta\phi \neq 0$ .

Figures 6(a)–6(f) show defect textures in symmetric and asymmetric geometries of a thick shell. The symmetric configuration shows two pairs of boojums at the poles of the inner and outer surfaces and a Saturn ring defect that encircles the inner surface in the nematic shell. In the asymmetric configuration, Saturn ring defects and boojums at the thick part of the nematic shell preserve their structures. However, the boojum core transforms from the single core to the split core with two short disclination curves ( $s = +1/2$ ) at the thin region [44]. The disclinations join together via a surface disclination ( $s = +1/2$ ) on the inner core. The final disclination is geometrically called the handle-shape defect [45,46], although it is energetically unstable. These disclinations are compatible with the planar anchoring on the outer shell but not with the conical anchoring on the inner; therefore the formation of surface disclinations is necessary.

In the absence of the saddle-splay elastic contribution, as shown in Figs. 6(g)–6(i), our calculations show four short disclination curves ( $s = +1/2$ ) that two-by-two make two handle shapes in the thin symmetric shells. The two handle shapes lie in perpendicular planes.

Present face-to-face boojum cores with axial symmetry in the thin shell increase the splay deformation around the surface point defects for equal elastic constants. In this regime, the director is perpendicular to the surfaces somewhere near the poles [see Fig. 6(b)]. The degenerate anchorings can decrease the cost of elastic deformations in the thin part of shells with the broken nematic axial symmetry. Therefore the director reorientation on surfaces gives rise to the single-core boojum in the thick shells and transforms into the split core boojum in the asymmetric and thin shells, as shown in Figs. 6(e) and 6(h).

#### IV. SUMMARY

We numerically investigated the spherical NLC shells in various thicknesses with degenerate conic and planar anchorings on the inner and outer surfaces, respectively. By studying the free energy behavior, we found that the symmetric nematic shells are favorable configurations for each thickness. This is a different result compared to planar anchoring on the surfaces where the inner particle tends to stand at the maximum asymmetry degree of the shell. Our calculations showed that the elastic deformations in the thick shells induce a pair of boojums and a surface Saturn ring defect on the inner surface, and a pair of boojums on the outer surface. In the thin shells, the boojums respectively transform to four bulk disclinations and two surface disclinations on the outer and inner surfaces of the nematic shell. According to the hypothetical proposition of Ref. [2], the handle-shape defect lines can provide two pairs of adjacent binding sites on the vertices of defects to make potential colloidal polymer chains with double bondings.

- 
- [1] A. S. Utada, E. Lorenceau, D. R. Link, P. D. Kaplan, H. A. Stone, and D. A. Weitz, *Science* **308**, 537 (2005).
  - [2] D. R. Nelson, *Nano Lett.* **2**, 1125 (2002).
  - [3] G. A. DeVries, M. Brunnbauer, Y. Hu, A. M. Jackson, B. Long, B. T. Neltner, O. Uzun, B. H. Wunsch, and F. Stellacci, *Science* **315**, 358 (2007).
  - [4] I. Musevic, M. Skarabot, U. Tkalec, M. Ravnik, and S. Zumer, *Science* **313**, 954 (2006).
  - [5] A. Fernandez-Nieves, V. Vitelli, A. S. Utada, D. R. Link, M. Marquez, D. R. Nelson, and D. A. Weitz, *Phys. Rev. Lett.* **99**, 157801 (2007).
  - [6] T. Lopez-Leon, V. Koning, K. B. S. Devaiah, V. Vitelli, and A. Fernandez-Nieves, *Nat. Phys.* **7**, 391 (2011).
  - [7] B. Senyuk, J. Aplinc, M. Ravnik, and I. I. Smalyukh, *Nat. Commun.* **10**, 1825 (2019).
  - [8] M. Škarabot, M. Ravnik, S. Žumer, U. Tkalec, I. Poberaj, D. Babič, N. Osterman, and I. Musevič, *Phys. Rev. E* **76**, 051406 (2007).
  - [9] U. Ognysta, A. Nych, V. Nazarenko, M. Škarabot, and I. Mušević, *Langmuir* **25**, 12092 (2009).
  - [10] B. Senyuk, Q. Liu, E. Bililign, P. D. Nystrom, and I. I. Smalyukh, *Phys. Rev. E* **91**, 040501(R) (2015).
  - [11] M. R. Mozaffari, M. Babadi, J. Fukuda, and M. R. Ejtehadi, *Soft Matter* **7**, 1107 (2011).
  - [12] S. R. Seyednejad, M. R. Mozaffari, T. Araki, and E. Nedaee Oskoe, *Phys. Rev. E* **98**, 032701 (2018).
  - [13] T. Araki and H. Tanaka, *Phys. Rev. Lett.* **97**, 127801 (2006).
  - [14] M. A. Bates, G. Skacej, and C. Zannoni, *Soft Matter* **6**, 655 (2010).
  - [15] D. Seč, T. Lopez-Leon, M. Nobili, C. Blanc, A. Fernandez-Nieves, M. Ravnik, and S. Žumer, *Phys. Rev. E* **86**, 020705(R) (2012).
  - [16] M. A. Gharbi, D. Seč, T. Lopez-Leon, M. Nobili, M. Ravnik, S. Žumer, and C. Blanc, *Soft Matter* **9**, 6911 (2013).
  - [17] S. R. Seyednejad, M. R. Mozaffari, and M. R. Ejtehadi, *Phys. Rev. E* **88**, 012508 (2013).
  - [18] V. Koning, T. Lopez-Leon, A. Darmon, A. Fernandez-Nieves, and V. Vitelli, *Phys. Rev. E* **94**, 012703 (2016).
  - [19] M. Sadati, Y. Zhou, D. Melchert, A. Guo, J. A. Martinez-Gonzalez, T. F. Roberts, R. Zhang, and J. J. de Pablo, *Soft Matter* **13**, 7465 (2017).
  - [20] Y. Ishii, Y. Zhou, K. He, Y. Takanishi, J. Yamamoto, J. De Pablo, and T. Lopez-Leon, *Soft Matter* **16**, 8169 (2020).
  - [21] M. Kleman and O. D. Lavrentovich, *Soft Matter Physics: An Introduction* (Springer, New York, 2003).
  - [22] I. I. Smalyukh, O. D. Lavrentovich, A. N. Kuzmin, A. V. Kachynski, and P. N. Prasad, *Phys. Rev. Lett.* **95**, 157801 (2005).

- [23] B. Senyuk, O. Puls, O. M. Tovkach, S. B. Chernyshuk, and I. I. Smalyukh, *Nat. Commun.* **7**, 10659 (2016).
- [24] O. O. Ramdane, P. Auroy, S. Forget, E. Raspaud, P. Martinot-Lagarde, and I. Dozov, *Phys. Rev. Lett.* **84**, 3871 (2000).
- [25] N. V. Madhusudana and K. R. Sumathy, *Mol. Cryst. Liq. Cryst.* **92**, 179 (1983).
- [26] V. Y. Rudyak, M. N. Krakhalev, V. S. Sutormin, O. O. Prishchepa, V. Y. Zyryanov, J.-H. Liu, A. V. Emelyanenko, and A. R. Khokhlov, *Phys. Rev. E* **96**, 052701 (2017).
- [27] Y. Zhou, B. Senyuk, R. Zhang, I. I. Smalyukh, and J. J. de Pablo, *Nat. Commun.* **10**, 1000 (2019).
- [28] P. Poulin and D. A. Weitz, *Phys. Rev. E* **57**, 626 (1998).
- [29] V. Bondar, D. Lavrentovich, and V. Pergamenschik, *J. Exp. Theor. Fiz.* **101**, 125 (1992).
- [30] T. Lopez-Leon and A. Fernandez-Nieves, *Phys. Rev. E* **79**, 021707 (2009).
- [31] G. E. Volovik and O. D. Lavrentovich, *J. Exp. Theor. Phys.* **85**, 1997 (1983).
- [32] H. Poincare, *J. Math. Pures Appl.* **1**, 167 (1885).
- [33] H. Hopf, *Math. Ann.* **96**, 225 (1927).
- [34] V. Vitelli and D. R. Nelson, *Phys. Rev. E* **74**, 021711 (2006).
- [35] G. Skačej and C. Zannoni, *Phys. Rev. Lett.* **100**, 197802 (2008).
- [36] M. N. Krakhalev, O. O. Prishchepa, V. S. Sutormin, and V. Y. Zyryanov, *Liq. Cryst.* **44**, 355 (2017).
- [37] S. R. Seyednejad, T. Araki, and M. R. Mozaffari, *Phys. Rev. E* **99**, 032702 (2019).
- [38] P. G. de Gennes and J. Prost, *The Physics of Liquid Crystal* (Oxford University Press, Oxford, England, 1995).
- [39] S. Kralj, S. Zumer, and D. W. Allender, *Phys. Rev. A* **43**, 2943 (1991).
- [40] H. Stark, *Phys. Rep.* **351**, 387 (2001).
- [41] J. B. Fournier and P. Galatola, *Europhys. Lett.* **72**, 403 (2005).
- [42] C. Geuzaine and J.-F. Remacle, *Int. J. Numer. Methods Eng.* **79**, 1309 (2009).
- [43] W. H. Press, S. A. Teukolsky, W. T. Vetterling, and B. P. Flannery, *Numerical Recipes*, 2nd ed. (Cambridge University Press, Cambridge, England, 1992).
- [44] M. Tasinkevych, N. M. Silvestre, and M. M. T. da Gama, *New J. Phys.* **14**, 073030 (2012).
- [45] Q. Liu, B. Senyuk, M. Tasinkevych, and I. I. Smalyukh, *Proc. Nat. Acad. Sci.* **110**, 9231 (2013).
- [46] M. G. Campbell, M. Tasinkevych, and I. I. Smalyukh, *Phys. Rev. Lett.* **112**, 197801 (2014).